Resolving Vibrational from Electronic Coherences in Two-Dimensional Electronic Spectroscopy: The Role of the Laser Spectrum

Franco V. de A. Camargo,[1,2] Lena Grimmelsmann,[1,3] Harry L. Anderson,[4] Stephen R. Meech,[1] and Ismael A. Heisler[1,*]
[1]School of Chemistry, Norwich Research Park, University of East Anglia, Norwich NR4 7TJ, United Kingdom
[2]CAPES Foundation, Ministry of Education of Brazil, Brasilia DF 70040-202, Brazil
[3]Fakultät für Chemie und Biochemie, Ruhr-Universität Bochum, Universitätsstrasse 150, 44801 Bochum, Germany
[4]Department of Chemistry, Chemistry Research Laboratory, University of Oxford, Oxford OX1 3TA, United Kingdom
(Received 24 August 2016; published 20 January 2017)

The observation of coherent quantum effects in photosynthetic light-harvesting complexes prompted the question whether quantum coherence could be exploited to improve the efficiency in new energy materials. The detailed characterization of coherent effects relies on sensitive methods such as two-dimensional electronic spectroscopy (2D-ES). However, the interpretation of the results produced by 2D-ES is challenging due to the many possible couplings present in complex molecular structures. In this work, we demonstrate how the laser spectral profile can induce electronic coherencelike signals in monomeric chromophores, potentially leading to data misinterpretation. We argue that the laser spectrum acts as a filter for certain coherence pathways and thus propose a general method to differentiate vibrational from electronic coherences.

DOI: 10.1103/PhysRevLett.118.033001

The development of two-dimensional electronic spectroscopy (2D-ES) enabled photophysical processes to be resolved with unprecedented temporal and spectral detail. The extra dimension, given by the excitation frequency axis, yields 2D spectra where discrimination of specific features (otherwise overlapped in 1D methods) is now possible [1]. Consequently, 2D-ES has provided new insights into topics as diverse as quantum phenomena in biology [2–4], energy transfer [5,6], singlet fission [7], nanomaterials [8,9], reaction dynamics [10–12], and many body effects in coupled quantum wells [13–15]. However, although 2D-ES greatly facilitates the discrimination of physical phenomena affecting electronic transitions such as line-broadening mechanisms, vibrational and electronic couplings, ambiguities remain in detailed analysis, especially for molecular systems where both vibrational and electronic couplings may play a role.

The observation of long-lived oscillations in 2D-ES measurements, assigned to coherent coupling between electronic transitions, in light harvesting systems sparked major interest, as it raised questions such as whether coherent effects could underlie the remarkably high efficiency of energy transfer in photosynthesis [16]. However, electronic transitions are commonly coupled to molecular vibrational modes, and vibrational coherences both in the ground and excited states can be prepared by broadband pulses, in the same way that a coherent superposition of different excitonic or electronic states may be prepared [17]. Recent theoretical and experimental research has explored the different coherence signatures arising in 2D-ES, but for the most part possible effects from the laser spectrum have been neglected [18–24].

In this Letter we study vibrational coherences in a zinc-porphyrin monomer (where electronic couplings are absent), and find that the laser spectrum content plays a crucial role in what is observed. We show that a laser spectrum with characteristics typical of those generally used in 2D-ES generates results that mimic the coherent evolution expected from a purely excitonic coupling scheme. This result is of critical importance in designing and interpreting 2D-ES experiments on coupled systems. We describe the physical origin of these results, and how such spectral filtering effects can be used in practice as a general method to unambiguously characterize vibrational coherences separately from other phenomena.

In order to study purely vibrational coherences in 2D-ES we chose a 5,15-bisalkynyl zinc porphyrin monomer [25], the normalized linear absorption of which is shown in Fig. 1. The lowest electronic transition in porphyrins is to a singlet state labeled the Q band and here it contains two peaks. The peak at 15650 cm^{-1} corresponds to the $Q_x(0-0)$ band [26], which is coupled to a zinc-pyrrole vibrational breathing mode of the porphyrin ring at 375 cm^{-1}, resulting in a vibronic shoulder at 16025 cm^{-1} [31]. The second absorption peak at higher energies ($\tilde{\nu} > 16500$ cm^{-1}) includes the $Q_y(0-0)$ transition and higher energy vibrational modes coupled to Q_x [32]. Thus, the electronic structure for $\tilde{\nu} < 16500$ cm^{-1} can be adequately described by a displaced harmonic oscillator model representing one electronic transition coupled to a single vibrational mode, as shown in Fig. 2(a).

We performed 2D-ES experiments using a conventional optics based scheme, outlined in the Supplemental Material [26], and detailed in Ref. [33]. 2D-ES requires determination of the excitation axis, which is possible by

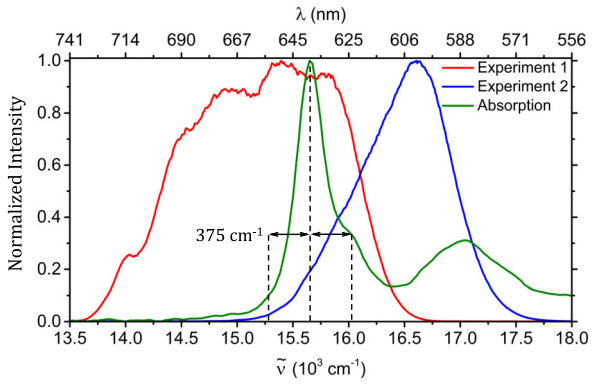

FIG. 1. Normalized linear absorption (green) and laser spectra used in experiments 1 (red) and 2 (blue). The sample was dissolved in n-pentane with 1 vol % of pyridine to a concentration of ~330 μM in a 200 μm path length static cell, corresponding to an optical density of 0.25 at 15650 cm^{-1} (639 nm).

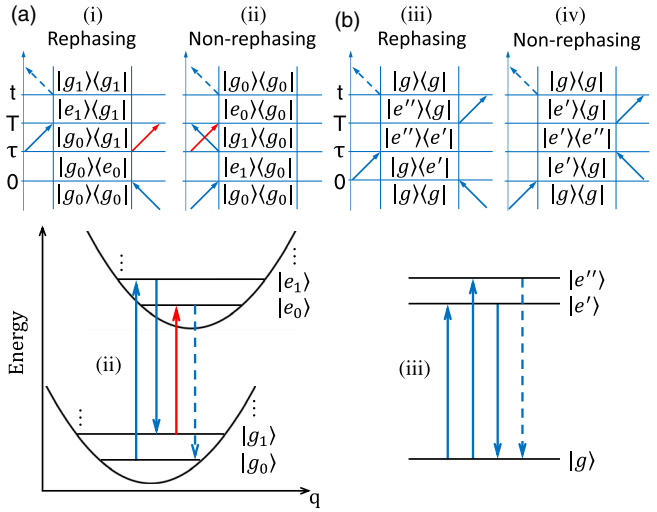

FIG. 2. (a) Examples of rephasing (i) and nonrephasing (ii) pathways with ground state coherences during T. The first arrow defines $\tilde{\nu}_1$, the dashed arrow is signal emission ($\tilde{\nu}_3$), and arrows connecting $|g_1\rangle$ to $|e_0\rangle$ are red. Below, pathway (ii) is drawn in a displaced harmonic oscillator energy level scheme. (b) Similar to (a), for an energy level with two electronic excited states. Here, pathways similar to (i) and (ii) are not possible, but in (a) pathways like (iii) and (iv) are.

experimentally controlling the time delay between the first and the second field-matter interactions (labeled τ-the coherence time), the Fourier pair of which is the excitation wave number $\tilde{\nu}_1$. Further, 2D-ES recovers the full complex-valued third-order polarization $P^{(3)}(\tilde{\nu}_1, T, \tilde{\nu}_3)$, which is the convolution of the system's third-order response function $S^{(3)}(\tilde{\nu}_1, T, \tilde{\nu}_3)$ with the electric fields [34], where the resolution of $\tilde{\nu}_1$ is defined only by the τ scanning range, and the temporal resolution along T (the population time) remains defined by the pulse duration [35]. As a result, 2D-ES recovers correlation maps between excitation and detection $(\tilde{\nu}_1, \tilde{\nu}_3)$ for each T. The 2D-ES signal arises from four-wave mixing pathways, which can be either rephasing (photon echo signal) or nonrephasing (free induction decay signal) according to their phase matching, and an equally weighted sum of both results in $P^{(3)}(\tilde{\nu}_1, T, \tilde{\nu}_3)$ [36,37]. Our experiment recovers complex-valued rephasing and nonrephasing maps independently [33,38].

In this work we are specifically concerned with four-wave mixing pathways that include vibrational coherences either in the ground or electronic excited states during T. For the displaced harmonic oscillator model, considering only the energy levels explicitly drawn in Fig. 2(a) there are 16 such pathways (Figs. S3–S7 display all [26]) and they generate oscillatory features in the data as a function of T. It is known that the phase of the oscillation due to each single pathway is a function of $(\tilde{\nu}_1, \tilde{\nu}_3)$, and that interference between neighboring contributions can generate confounding features, so isolation of as few pathways as possible is helpful for proper interpretation of the data [18,38]. To that end, we note that eight of the coherence pathways are rephasing, while the other eight are nonrephasing. Further, we note that the oscillatory behavior arises from the systems' density matrix being in a coherence (such as $|g_0\rangle\langle g_1|$ or $|g_1\rangle\langle g_0|$) during T. The density matrix is a Hermitian operator, so $|g_0\rangle\langle g_1| = |g_1\rangle\langle g_0|^*$, and therefore, if $|g_0\rangle\langle g_1|$ modulates the third order response as $e^{+i\nu_0 T}$, then $|g_1\rangle\langle g_0|$ will modulate the response as $e^{-i\nu_0 T}$, where $\nu_0 > 0$. Consequently, beatings arising from $|g_0\rangle\langle g_1|$ and $|g_1\rangle\langle g_0|$ coherences during T will be observed with opposite frequency signs when the complex-valued spectra are Fourier transformed [39]. Thus, we can sort the pathways for each of rephasing and nonrephasing signals according to $\tilde{\nu}_1$ (first arrow), $\tilde{\nu}_3$ (dashed arrow), and the frequency sign during T, obtaining Figs. 3(a) and 3(b). Significantly, rephasing negative [Fig. 3(a), red symbols] and nonrephasing positive [Fig. 3(b), green symbols] frequencies include only two pathways, each forming two peaks, all corresponding to vibrational coherences in the electronic excited state [40]. The remaining six pathways for both rephasing and nonrephasing have frequencies with opposite sign and are arranged in four peaks [Figs. 3(a) and 3(b)].

The first set of measurements was performed using the laser spectrum displayed in red in Fig. 1. This spectrum fully covers the lowest peak in the sample's linear absorption and also has significant bandwidth towards lower energies. Our 2D-ES setup allows fast acquisition of complex-valued rephasing and nonrephasing spectra, enabling us to scan T from 30 to 1000 fs with time steps of 5 fs, yielding 196 spectra of each type. These maps include not only the oscillatory pathways discussed above, but also an equal number of nonoscillatory ones, which are associated with population dynamics [26]. In order to remove nonoscillatory amplitude, we stack together 2D-ES maps for all values of T and globally fit the data with exponential decays, so that the

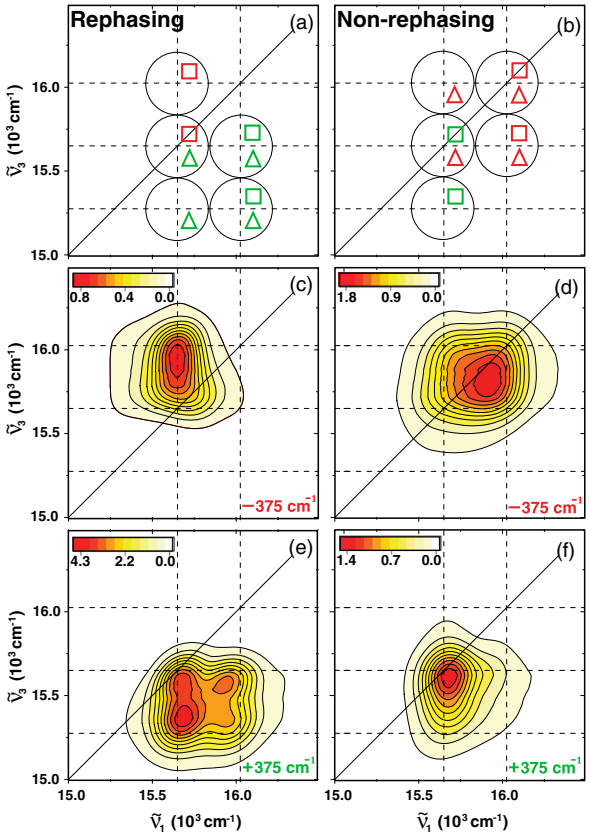

FIG. 3. (a) Diagrammatic scheme representing the positions of the rephasing oscillatory pathways in the $(\tilde{\nu}_1, \tilde{\nu}_3)$ plane. Each oscillatory pathway is marked with an open geometric figure, with triangles and squares representing vibrational coherences in the electronic ground and excited states, respectively. Red and green symbols represent pathways of negative and positive frequency, respectively, and the 2D-ES signal from each pathway is centered on the black circle around them. (b) Same as (a) for nonrephasing. (c)–(f) Experimentally obtained oscillation amplitude maps for $\tilde{\nu}_2 = -375$ cm^{-1} in rephasing (c) and nonrephasing (d) measurements, and $\tilde{\nu}_2 = +375$ cm^{-1} in rephasing (e) and nonrephasing (f) in experiment 1.

residuals from this fit will consist only of the coherent oscillations [41]. We then perform a Fourier transform of the complex-valued residuals of rephasing and nonrephasing signals over T for every $(\tilde{\nu}_1, \tilde{\nu}_3)$ pair, thus recovering the oscillatory amplitude for any given wave number $\tilde{\nu}_2$ within the Nyquist limit. By selecting a specific value of $\tilde{\nu}_2$, we can plot the corresponding amplitude as a function of $(\tilde{\nu}_1, \tilde{\nu}_3)$, which is called an oscillation amplitude map [42]. Because they include only the oscillatory amplitude at the selected value of $\tilde{\nu}_2$, they are analogous to the schemes in Figs. 3(a) and 3(b). The experimental oscillation amplitude maps at $\tilde{\nu}_2 = \pm 375$ cm^{-1} are shown in Figs. 3(c)–3(f). We observe good agreement between experimental results and the predictions in Figs. 3(a) and 3(b). For example, Fig. 3(e) has four peaks forming a square approximately in the positions marked by the green symbols in Fig. 3(a), while Fig. 3(c) shows amplitude elongated along the positions marked by the red symbols in Fig. 3(a). Such agreement confirms that the experiment is capable of resolving positive from negative frequencies (see Fig. S15 for typical time domain data [26]). Even though we maximized the isolation of pathways, overlap between neighboring contributions in the $(\tilde{\nu}_1, \tilde{\nu}_3)$ plane remains, leading to the convoluted nature of the peaks and small shifts from the predicted $(\tilde{\nu}_1, \tilde{\nu}_3)$ coordinates [38].

These oscillation maps contrast with those expected for an electronically coupled system with energy levels shown in Fig. 2(b), in which case the absence of a second energy level in the ground state significantly reduces the number of pathways. For instance, coherence pathways analogous to (iii) and (iv) in Fig. 2(b) are possible in the vibrational case, but those represented by (i) and (ii) cannot exist in the pure electronic coupling case, as they require a sublevel in the ground state [18]. In the electronic case only four coherence pathways remain, with two oscillatory peaks in the diagonal in nonrephasing maps, and two in the off-diagonal in rephasing maps [26]. Thus, the collective presence of pathways in either this pattern or that from Figs. 3(c)–3(f) is a good criterion to distinguish purely vibrational from purely electronic coherences [43].

At this point, we emphasize that there is a significant difference between the present experiment and the usual cases in 2D-ES. Here, the molecule's absorption peak is sufficiently narrow to be fully covered by the laser spectrum with substantial bandwidth remaining on the low energy side. Most systems of interest with absorption in the visible region possess much broader absorption peaks, which are challenging to cover even with the shortest available pulses. Thus, a typical 2D-ES experiment centers the laser spectrum around the absorption region of interest, leaving little bandwidth to lower wave numbers than the pure electronic transition, where there is no absorption. Since the early days in ultrafast spectroscopy authors have been aware of potential effects due to the laser spectrum [44], and seminal 2D-ES studies concluded it merely acts as a filter on the $\tilde{\nu}_1$ and $\tilde{\nu}_3$ axes [45,46], which was experimentally confirmed [21]. However, these studies focused on 2D-ES maps for a single T, not discussing coherent signatures. Therefore, we performed a second set of 2D-ES measurements using the spectrum shown in blue in Fig. 1, once again selecting only the oscillatory features at 375 cm^{-1} using the same procedure as for Fig. 3 [26].

To discuss the results expected for experiment 2, we note that although the spectrum fully covers the lowest absorption peak, it has almost no amplitude at 15275 cm^{-1}, corresponding to a transition between $|e_0\rangle$ and $|g_1\rangle$ [see Figs. 1 and 2(a)]. It follows that the oscillatory features with detection at 15275 cm^{-1} will be suppressed, as the detection axis $(\tilde{\nu}_3)$ range is defined by the laser spectrum. Regarding the excitation axis $(\tilde{\nu}_1)$, it is defined by the first field-matter interaction, which can only happen at a

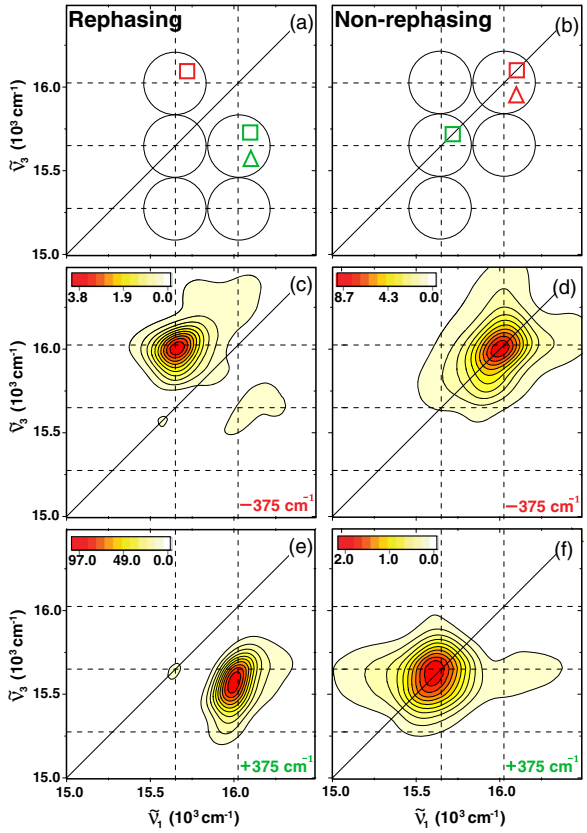

FIG. 4. Same as Fig. 3 for experiment 2.

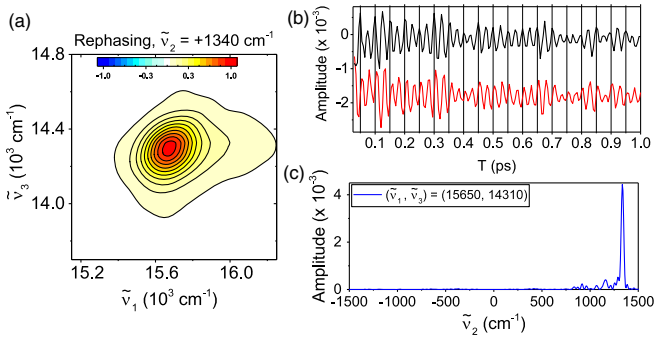

FIG. 5. (a) Oscillation amplitude map at $\tilde{\nu}_2 = 1340\ \mathrm{cm}^{-1}$. (b) Real (black) and imaginary (red) rephasing amplitude at $\tilde{\nu}_1 = 15650\ \mathrm{cm}^{-1}$ and $\tilde{\nu}_3 = 14310\ \mathrm{cm}^{-1}$ in experiment 1. (c) Power spectrum of the fit residuals at the same position. The amplitude at negative frequencies is negligible and the smaller peaks arise from Raman modes of *n*-pentane [47].

frequency that the molecule absorbs. Therefore, because all absorption is still covered by the laser, there is no effect on this axis. From these considerations, it is tempting to merely exclude the peaks detected at 15275 cm^{-1} from Fig. 3 and consider the rest will remain unaltered. However, 2D-ES signals arise from three field-matter interactions before signal emission, and all interactions must be at frequencies covered by the laser spectrum. This requires the exclusion of all pathways for which any of the field-matter interactions take place at a frequency not present in the laser spectrum. For example, pathways (i) and (ii) shown in Fig. 2(a) are both suppressed because an intermediate field-matter interaction (red arrows) takes place at 15275 cm^{-1}, even though excitation and detection frequencies lie within the laser spectrum. This plays an important role regarding which vibrational coherences are detected in 2D-ES experiments. The coherence pathways with all interactions wholly within the laser spectrum of experiment 2 are represented in Figs 4(a) and 4(b). The surprising result is not only that the remaining oscillatory peaks are diagonal for nonrephasing and off-diagonal for rephasing, but also that the frequency sign of the oscillation is the same as that expected for a purely electronic coherence (see Fig. S11 [26]). The experimental result in Figs 4(c)–4(f) confirms this forecast. Therefore, in a typical realization of a 2D study in the visible region, a vibrational mode coupled to an electronic transition may generate the same pattern of oscillatory features as an electronic coherence, leading to a potentially misleading interpretation.

The key issue is that a spectrum like that of experiment 1, covering a vibrational quantum on both sides of the main absorption, is often unattainable in practice, so only a spectrum similar to experiment 2 is used. Having understood the role of the laser spectrum allows us to go one step further and consider a new experiment, using a redshifted laser spectrum that covers the transitions between $|g_0\rangle$ and $|e_0\rangle$, and between $|e_0\rangle$ and $|g_1\rangle$, but fails to cover the transition between $|g_0\rangle$ and $|e_1\rangle$. This means that the vibronic peak in the linear absorption is not covered, and therefore no coherences in the electronic excited state can be prepared (as an excitation to $|e_1\rangle$ would be required). Nonetheless, systematic analysis shows that two coherence pathways in the ground state remain: one nonrephasing, analogous to that represented in Fig. 3(b) as a red triangle at $\tilde{\nu}_1 = \tilde{\nu}_3 = 15650\ \mathrm{cm}^{-1}$, and one rephasing, analogous to the green triangle at $\tilde{\nu}_1 = 15650\ \mathrm{cm}^{-1}$ and $\tilde{\nu}_3 = 15275\ \mathrm{cm}^{-1}$ in Fig. 3(a) (see Fig. S9 [26]).

To test this, we note that the porphyrin monomer is known to have a vibrational mode at 1340 cm^{-1} coupled to Q_x, which for experiment 1 falls exactly in this regime: the vibronic peak in the linear absorption is at 16990 cm^{-1} [32], where there is no laser intensity, but intensity is available at $\tilde{\nu}_3 = 15650 - 1340\ \mathrm{cm}^{-1} = 14310\ \mathrm{cm}^{-1}$. Figure 5 shows the rephasing oscillation amplitude map at $\tilde{\nu}_2 = +1340\ \mathrm{cm}^{-1}$ with the scale zoomed around $\tilde{\nu}_3 = 14310\ \mathrm{cm}^{-1}$, and a peak is indeed detected. Figures 5(b) and 5(c) show the time and frequency domain data at this coordinate, confirming the expected oscillation. We emphasize that the rephasing amplitude of this oscillation is smaller than 0.4% of the maximum signal, but can still be resolved because it is a cross peak in a mostly background free region. In the nonrephasing diagonal, where the other pathway is expected, the signal to noise ratio of our measurement was insufficient to detect this oscillation.

In conclusion, the present results deepen the understanding on how to detect and interpret coherent oscillations in 2D-ES measurements, highlighting the fact that for complex energy level structures, the laser spectrum plays a crucial and nontrivial role regarding the oscillations detected. We have demonstrated that a redshifted laser spectrum can be used to selectively prepare coherences in the ground state, thus complementing experiments where the spectrum causes the ambiguity we reported. The effect of the laser spectrum on coherences has been recently discussed in the literature, but the filtering effect was not discussed [48]. The selection of specific pathways through two-color experiments has also been described [49–51], but the concept that some vibronic signatures may be missing in one-color experiments, as described here, was previously only briefly noted by Butkus *et al.* [52]. Recently, there have been efforts to model excitonic systems with the inclusion of vibrational coupling, giving rise to more complex energy level structures [53], which were experimentally verified in an artificial light harvesting complex whose structure proved especially convenient for rigorous polarization experiments [54]. For the study of other complex systems, our results demonstrate that explicit inclusion of the laser spectrum is essential for rigorous design and interpretation of 2D-ES experiments, and show how the laser spectrum can be used as a tool to fully benchmark ground-state coherences.

This work was supported by Engineering and Physical Sciences Research Council Grants No. EP/J009148/1 and No. J021431/1. F. V. A. C. thanks Brazilian Funding Agency Coordination for the Improvement of Higher Level -or Education- Personnel for support in his doctoral studentship (BEX 9527/13-3). L. G. thanks the Cluster of Excellence RESOLV (EXC 1069) funded by the Deutsche Forschungsgemeinschaft for financial support. We thank Professor Darius Abramavicius and Dr. Vytautas Butkus for useful discussions, and Dr. Martin D. Peeks for synthesizing the porphyrin monomer used in this work.

*i.heisler@uea.ac.uk

[1] J. D. Hybl, A. W. Albrecht, S. M. Gallagher Faeder, and D. M. Jonas, Chem. Phys. Lett. **297**, 307 (1998).
[2] H. Lee, Y.-C. Cheng, and G. R. Fleming, Science **316**, 1462 (2007).
[3] G. S. Engel, T. R. Calhoun, E. L. Read, T. K. Ahn, T. Mancal, Y. C. Cheng, R. E. Blankenship, and G. R. Fleming, Nature (London) **446**, 782 (2007).
[4] E. Collini, C. Y. Wong, K. E. Wilk, P. M. G. Curmi, P. Brumer, and G. D. Scholes, Nature (London) **463**, 644 (2010).
[5] E. Thyrhaug, K. Žídek, J. Dostál, D. Bína, and D. Zigmantas, J. Phys. Chem. Lett. **7**, 1653 (2016).
[6] E. Collini and G. D. Scholes, Science **323**, 369 (2009).
[7] A. A. Bakulin, S. E. Morgan, T. B. Kehoe, M. W. B. Wilson, A. W. Chin, D. Zigmantas, D. Egorova, and A. Rao, Nat. Chem. **8**, 16 (2016).
[8] E. Cassette, J. C. Dean, and G. D. Scholes, Small **12**, 2234 (2016).
[9] T. Stoll, E. Sgrò, J. W. Jarrett, J. Réhault, A. Oriana, L. Sala, F. Branchi, G. Cerullo, and K. L. Knappenberger, J. Am. Chem. Soc. **138**, 1788 (2016).
[10] P. Nuernberger, S. Ruetzel, and T. Brixner, Angew. Chem., Int. Ed. Engl. **54**, 11368 (2015).
[11] S. Ruetzel, M. Kullmann, J. Buback, P. Nuernberger, and T. Brixner, Phys. Rev. Lett. **110**, 148305 (2013).
[12] F. V. A. Camargo, H. L. Anderson, S. R. Meech, and I. A. Heisler, J. Phys. Chem. B **119**, 14660 (2015).
[13] K. W. Stone, K. Gundogdu, D. B. Turner, X. Li, S. T. Cundiff, and K. A. Nelson, Science **324**, 1169 (2009).
[14] G. Nardin, G. Moody, R. Singh, T. M. Autry, H. Li, F. Morier-Genoud, and S. T. Cundiff, Phys. Rev. Lett. **112**, 046402 (2014).
[15] G. Moody, I. A. Akimov, H. Li, R. Singh, D. R. Yakovlev, G. Karczewski, M. Wiater, T. Wojtowicz, M. Bayer, and S. T. Cundiff, Phys. Rev. Lett. **112**, 097401 (2014).
[16] A. Chenu and G. D. Scholes, Annu. Rev. Phys. Chem. **66**, 69 (2015).
[17] N. Christensson, F. Milota, J. Hauer, J. Sperling, O. Bixner, A. Nemeth, and H. F. Kauffmann, J. Phys. Chem. B **115**, 5383 (2011).
[18] V. Butkus, D. Zigmantas, L. Valkunas, and D. Abramavicius, Chem. Phys. Lett. **545**, 40 (2012).
[19] V. Butkus, D. Zigmantas, D. Abramavicius, and L. Valkunas, Chem. Phys. Lett. **587**, 93 (2013).
[20] T. Mancal, N. Christensson, V. Lukes, F. Milota, O. Bixner, H. F. Kauffmann, and J. Hauer, J. Phys. Chem. Lett. **3**, 1497 (2012).
[21] J. R. Caram, A. F. Fidler, and G. S. Engel, J. Chem. Phys. **137**, 024507 (2012).
[22] A. Chenu, N. Christensson, H. F. Kauffmann, and T. Mancal, Sci. Rep. **3**, 2029 (2013).
[23] V. Perlík, C. Lincoln, F. Šanda, and J. Hauer, J. Phys. Chem. Lett. **5**, 404 (2014).
[24] E. Cassette, R. D. Pensack, B. Mahler, and G. D. Scholes, Nat. Commun. **6**, 6086 (2015).
[25] D. Koszelewski, A. Nowak-Krol, M. Drobizhev, C. J. Wilson, J. E. Haley, T. M. Cooper, J. Romiszewski, E. Gorecka, H. L. Anderson, A. Rebane, and D. T. Gryko, J. Mater. Chem. C **1**, 2044 (2013).
[26] See Supplemental Material at http://link.aps.org/supplemental/10.1103/PhysRevLett.118.033001, which includes Refs. [27–30], for sample's chemical structure and linear absorption, a brief description of the two-dimensional electronic spectroscopy experimental (2D-ES) setup and a complete list of Liouville-space pathways. Typical real and imaginary rephasing and nonrephasing 2D-ES maps and typical time-traces containing coherent oscillations of positive and negative frequencies are provided for all reported experiments.
[27] F. D. Fuller and J. P. Ogilvie, Annu. Rev. Phys. Chem. **66**, 667 (2015).
[28] U. Selig, F. Langhojer, F. Dimler, T. Loehrig, C. Schwarz, B. Gieseking, and T. Brixner, Opt. Lett. **33**, 2851 (2008).
[29] M. L. Cowan, J. P. Ogilvie, and R. J. D. Miller, Chem. Phys. Lett. **386**, 184 (2004).

[30] V. Butkus, D. Abramavicius, A. Gelzinis, and L. Valkunas, Lith. J. Phys. **50**, 267 (2010).
[31] M. Atamian, R. J. Donohoe, J. S. Lindsey, and D. F. Bocian, J. Phys. Chem. **93**, 2236 (1989).
[32] M. Drobizhev, Y. Stepanenko, Y. Dzenis, A. Karotki, A. Rebane, P. N. Taylor, and H. L. Anderson, J. Phys. Chem. B **109**, 7223 (2005).
[33] I. A. Heisler, R. Moca, F. V. A. Camargo, and S. R. Meech, Rev. Sci. Instrum. **85**, 063103 (2014).
[34] A. Tokmakoff, J. Phys. Chem. A **104**, 4247 (2000).
[35] P. Hamm and M. Zanni, *Concepts and Methods of 2D Infrared Spectroscopy* (Cambridge University Press, Cambridge, England, 2011).
[36] M. Khalil, N. Demirdöven, and A. Tokmakoff, Phys. Rev. Lett. **90**, 047401 (2003).
[37] M. Khalil, N. Demirdöven, and A. Tokmakoff, J. Phys. Chem. A **107**, 5258 (2003).
[38] F. V. A. Camargo, H. L. Anderson, S. R. Meech, and I. A. Heisler, J. Phys. Chem. A **119**, 95 (2015).
[39] J. Seibt and T. Pullerits, J. Phys. Chem. C **117**, 18728 (2013).
[40] Y. Song, C. Hellmann, N. Stingelin, and G. D. Scholes, J. Chem. Phys. **142**, 212410 (2015).
[41] V. I. Prokhorenko, EPA Newsl. (Print), 21 (2012).
[42] D. B. Turner, R. Dinshaw, K.-K. Lee, M. S. Belsley, K. E. Wilk, P. M. G. Curmi, and G. D. Scholes, Phys. Chem. Chem. Phys. **14**, 4857 (2012).
[43] Y.-C. Cheng and G. R. Fleming, J. Phys. Chem. A **112**, 4254 (2008).
[44] A. Lorincz, F. A. Novak, and S. A. Rice, Chem. Phys. Lett. **111**, 322 (1984).
[45] S. M. G. Faeder and D. M. Jonas, J. Phys. Chem. A **103**, 10489 (1999).
[46] P. Kjellberg, B. Bruggemann, and T. Pullerits, Phys. Rev. B **74** (2006).
[47] C. D. Keefe and S. Jaspers-Fayer, Vib. Spectrosc. **57**, 72 (2011).
[48] R. Tempelaar, A. Halpin, P. J. M. Johnson, J. Cai, R. S. Murphy, J. Knoester, R. J. D. Miller, and T. L. C. Jansen, J. Phys. Chem. A **120**, 3042 (2016).
[49] D. Abramavicius, V. Butkus, J. Bujokas, and L. Valkunas, Chem. Phys. **372**, 22 (2010).
[50] S. S. Senlik, V. R. Policht, and J. P. Ogilvie, J. Phys. Chem. Lett. **6**, 2413 (2015).
[51] J. O. Tollerud, C. R. Hall, and J. A. Davis, Opt. Express **22**, 6719 (2014).
[52] V. Butkus, A. Gelzinis, R. Augulis, A. Gall, C. Büchel, B. Robert, D. Zigmantas, L. Valkunas, and D. Abramavicius, J. Chem. Phys. **142**, 212414 (2015).
[53] V. Tiwari, W. K. Peters, and D. M. Jonas, Proc. Natl. Acad. Sci. U.S.A. **110**, 1203 (2013).
[54] J. Lim, D. Paleček, F. Caycedo-Soler, C. N. Lincoln, J. Prior, H. von Berlepsch, S. F. Huelga, M. B. Plenio, D. Zigmantas, and J. Hauer, Nat. Commun. **6**, 7755 (2015).